

V350 Muscae: RR Lyrae Star Distance Estimate and RRab Reclassification

Demetris Nicolaides

Natural Science and Mathematics, Bloomfield College, 467 Franklin Street, Bloomfield, NJ 07003; demetris_nicolaides@bloomfield.edu

Destiny L. King

Bloomfield College, 467 Franklin Street, Bloomfield, NJ 07003

Sandra Moreno Cristobal

Gardner-Webb University, 110 S. Main Street, Boiling Springs, NC 28017

Received December 15, 2020; revised January 15, 27, 2021; accepted February 15, 2021

Abstract V350 Mus was observed in the B, V, and, for the first time, the i and z bands, for a total of eighteen days. The telescope images were processed through aperture photometry. The star’s light curves reclassified it as an RRab type from its previous RRc or EW (eclipsing variable) classification. Its pulsation period was 0.3705 ± 0.0012 day. Three theoretical period-luminosity-metallicity relations of RR Lyrae stars (M_v , M_i , and M_z), were shown to collectively work quite well with the corresponding observed apparent magnitudes of V350 Mus in matching its Gaia reported distance of (165.34 ± 1) parsecs. Specifically, the distance estimates (in parsecs) for the V, i, and z filters were 145.70 ± 11 , 172.14 ± 7 , and 176.70 ± 7 , respectively, with their average being 164.85 ± 5 , a mere 0.30% difference from the Gaia value. The calculation of the three-filter average distance was optimum when A, the extinction factor due to galactic reddening, was calibrated by implementing a simple new formula that considers the amount of each wavelength’s extinction proportionally, by balancing it with respect to the extinction of an average wavelength (instead of, say with respect to the extinction of only the V wavelength). The type of average wavelength that worked best was the weighted mean of the wavelengths that have a period-luminosity-metallicity relation (in our study, the V, i, and z wavelengths), and where the weight of a particular band wavelength was its ratio to an arbitrary reference wavelength.

1. Introduction

We measured the time variation of the apparent magnitude of V350 Mus, its period of pulsation, and constructed its light curves for the B, V, i, and z bands. These data were then inserted in three theoretical RR Lyrae period-luminosity-metallicity relations, the M_v (Catelan *et al.* 2004), and the M_i and M_z (Cáceres and Catelan 2008) in order to calculate the star’s absolute magnitudes for each band and in turn estimate the corresponding distances. If verified, these relations can be used to calculate absolute magnitudes, thus providing an additional method in the determination of distances for RR Lyrae stars, and consequently enriching the cosmic distance ladder methodology of astronomy. Alternatively, these period-luminosity-metallicity relations may be used in “reverse”: from an RR Lyrae star’s known distance, apparent magnitude, and period, these relations can be applied to generate such star’s extinction factor, A, and reddening value, $E(B-V)$.

Pulsating stars have interesting and unique properties (Catelan and Smith 2014). In 1908, astronomer Henrietta Leavitt (Leavitt 1908) discovered the first period-luminosity relation of pulsating stars, the Cepheids in particular, which allowed for a new and improved method for measuring cosmic distances. Her work was seminal. Not only it is the basis of this paper and of an immense number of other ones that deal with variable stars—including Gaia Collab. *et al.* (2017)—it was also crucial in the work of Edwin Hubble (Hubble 1929) when he measured distances and recession velocities of distant galaxies and confirmed the expansion of the universe that was previously predicted theoretically by the field equations of Einstein’s general relativity.

V350 Mus (Figure 1) is a relatively nearby object, in the Milky Way’s disk. The star hasn’t been studied in the i and z filters previously. Table 1 lists its basic properties.

Table 1. Basic Properties of V350 Mus.

R. A. (°)	203.105
Dec. (°)	−74.61
Plx (mas)	6.0193
Glon (°)	305.698
Glat (°)	−11.959
pmRA (mas/yr)	−5.59
pmDE (mas/yr)	23.337
T_{eff} (K)	6356.19
distance ¹ (parsec)	165.34 ± 1
[Fe/H] ² (dex)	0.14
Flux B ³ (mag)	8.70 ± 0.02
Flux V ³ (mag)	8.23 ± 0.01
VarType ⁴	RRc ⁴ /EW ⁵
P ⁶ (d)	0.73811
P ⁷ (d)	0.36905
SpecType ⁸	F2IV

* Our study reclassified V350 Mus as an RRab. Note: the properties without a superscript are from (Gaia *et al.* 2018). ¹Bailer-Jones *et al.* 2018. ²Ammons *et al.* 2006; the Ammons paper estimated the value of 0.14 from polynomials of broadband photometry (although the authors wrote their code to derive [Fe/H] values using dwarf stars, not RR Lyrae); the 1σ error in this value is $\sigma[\text{Fe}=\text{H}] = +0.15 / -0.16$ dex (found in the VizieR Online Data Catalog: T_{eff} and metallicities for Tycho-2 stars (Ammons *et al.* 2006)). ³Hog *et al.* 2000. ⁴Watson *et al.* 2006; Kazarovets *et al.* 2011; Samus *et al.* 2017. ⁵Watson *et al.* 2014; Astraatmadja and Bailer-Jones 2016. ⁶Astraatmadja and Bailer-Jones 2016; the reference that reports this period classifies the star as EW. ⁷Watson *et al.* 2006; the reference that reports this period classifies the star as RRc. ⁸Schlafly *et al.* 2019.

2. Observations and methods

The observations of V350 Mus were completed at the Siding Spring Observatory (New South Wales, Australia) and at the South African Astronomical Observatory (Sutherland, South Africa), by three 0.4-meter SBIG robotic telescopes. The observatories are part of a global network with its Headquarters at Las Cumbres Observatory (LCO). The CCD camera of such a telescope (Brown *et al.* 2013) has 2048×3072 pixels, each of which has a 0.57-arcsecond square view of the sky, resulting in a total Field of View (FoV) of 19×29 arcminutes.

These observations lasted a total of 18 days in June and July 2020. The June 12–16 observations were adjusted for a simple period cadence with period=4.5 h and jitter=4.5 h; for June 16–24, period=2.9 h, jitter=2.9 h; and July 1–5, period=1.9 h, jitter=1.9 h. The observations were done in the Bessel-B, Bessel-V, SDSS-i, and PANSTARRS-z filters, with wavelength center (Å) 4361, 5448, 7545, and 8700, respectively. The exposure times of each filter were: 8 sec for B; 3 sec for V; 3 sec for i; and 12 sec for z. These values were calculated based on a test observation with exposure times 12 sec for B, V, and i, and 30 sec for z. The adjusted exposure times aimed for 300,000 counts (photoelectrons) of apparent magnitude and were achieved by using the software *ASTROIMAGEJ* (Collins *et al.* 2017). Figure 1 shows a typical colored image of the star field with V350 Mus in the center. Since a star's position changes with time, the most up-to-date coordinates of V350 Mus (R. A. = 203.10438°, Dec. = -74.60996°) were obtained with the use of one such image and the software *Aladin* (Bonnarel *et al.* 2000): we zoomed into the star, visually centered the cursor in the star image, and read off its coordinates. We used these coordinates for our analysis.

The images from the observatories were transmitted to Las Cumbres' Our Solar Siblings for processing by its data pipeline (Fitzgerald 2018). In addition to the fits files, the pipeline also generated the following two types of files: phototif (digital-camera-like images) and phot (the apt, sek, sex, dao, dop, and psx photometric procedures). These files were then forwarded to the google drives of the research team.

First, we visually inspected the phototif images of each filter and noted the unsuccessful ones—observations that occurred during a cloudy or windy night, or during excess light from the presence of the moon, or generally overexposed images with visible diffraction imperfections. We then eliminated all such images from each phot file. We cleaned further the phot images by also eliminating those with the smallest size (initially the ones up to 3 KB) as these were the images with the least number of stars detected in the specified field of view. (A good image is generally one that contains many stars for comparison purposes with catalogued stars and a target star.) The light curves of each filter in each of the six photometric analyses were constructed by running *astrosorce* (in *Spyder/Anaconda*). To calibrate the comparison stars for the B and V observations, *astrosorce* uses the APASS catalogue (Henden *et al.* 2016), but for the i and z observations (and since V350 Mus is in the southern hemisphere), *astrosorce* used the *Skymapper DR1.1* catalogue (Wolf *et al.* 2018).

The images of V350 Mus (see, for example, Figure 1)

showed a rather isolated star and so we expected any of the aperture photometry procedures (apt, sek, sex files) to produce more reliable results compared to any of the point spread function (PSF) photometry procedures (dop, dao, psx), which are more appropriate for images with many and overlapping stars. The sek (Source Extractor Kron) procedure (Bertin and Arnouts 1996) provided the best light curves. The cleaned sek images were cleaned even further as follows: in the B filter we kept images of 5 KB and up; in the i, 11 KB and up; in the V, 8 KB and up; and in the z, 9 KB and up. This additional cleaning provided consistency in the shape of the light curves of each band (Figures 2–5)—showing a rather steep ascent with a more gradual descent, a characteristic of RRab Lyrae stars—as well as consistency in the values of the most likely periods in the brightness variation. This cleaning, however, also produced a bit of inaccuracy in the values of the amplitudes (Table 2)—these are usually expected to decrease with increasing wavelength. Gaps in the light curves (from the cleaning process) can generate biased amplitudes.

The periods were calculated from two methods, the PDM (phase dispersion minimization) and the string method. The *astrosorce* routine, in search of the most probable period for each filter and for each method, was written by Altunin *et al.* (2020) by basing their work on the PDM method, first developed by Stellingwerf (1978), and on the string method, first developed by Dworetzky (1983). In the PDM method, for each probable period, the points of the corresponding potential light curve are imagined grouped in vertical bins. Each such bin choice contains, therefore, its own unique set of dispersed points. The most probable period (and thus best light curve) is produced when the dispersion of the points in each bin is minimal. In the string method, for each probable period, the points of the corresponding potential light curve are imagined connected sequentially with a string. The most probable period generates the smallest total string length and the best light curve.

3. Results and calculations

3.1. Measurements

The star's light curves, particularly that in the V filter, (Figures 2–5) reclassified it as an RRab type from its previous RRc (Watson *et al.* 2006; Kazarovets *et al.* 2011; Samus *et al.* 2017), or EW (eclipsing variable) classification (Watson *et al.* 2014; Astraatmadja and Bailer-Jones 2016). Table 2 includes the amplitude of each light curve and the most probable periods for each wavelength (from the string and PDM methods), as well as the average of these periods. All eight most likely periods were within each other's uncertainty. This table has also the mid-range value of the measured apparent magnitude, *m*, which is decreasing from the shorter wavelength, B, to the longer, i, (as expected, for example, by Rayleigh scattering, according to which more “blue” than “red” scatters off the main beam of the star and thus doesn't reach the telescope), although not from i to z. Amplitudes are relatively low in all filters, and we note that we do not see the usual decrease in amplitude in going from B to i. While such an effect can sometimes arise when an RR Lyrae star image is blended with that of a nonvariable star, we do not see evidence of such a blend in our images.

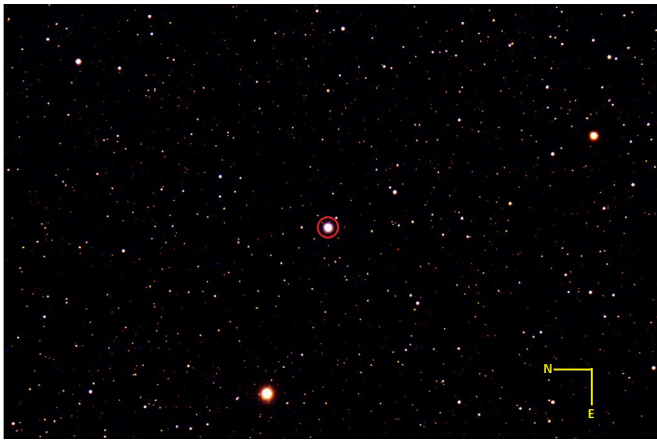


Figure 1. V350 Mus (enclosed by the red circle) is the brightest star in the middle of this RGB image processed from one representative image from each filter used. North is left; east is down.

Table 2. Apparent magnitudes, periods, and amplitudes of V350 Mus.

	Band			
	B	V	i	z
λ -ctr (Å)	4361	5448	7545	8700
m^a (mag)	8.300	7.927	7.838	7.869
errm (mag)	0.035	0.015	0.010	0.012
P^b (d)	0.3699	0.3715	0.3706	0.3708
err P^b (d)	0.0044	0.0044	0.0046	0.0033
P^c (d)	0.3695	0.3716	0.3702	0.3702
err P^c (d)	0.0032	0.0036	0.0016	0.0029
P -avg $\equiv P$ (d)		0.3705 \pm 0.0012		
Amp d (mag)	0.336	0.324	0.413	0.374

^a $m = (m_{max} + m_{min})/2$. ^bUsing the string method. ^cUsing the PDM method. ^dAmp = $(m_{max} - m_{min})$.

3.2. Preliminary calculations

The theoretical period-luminosity-metallicity relations that are being tested in this paper, as to whether they generate the right distance of V350 Mus, are:

$$M_v = 2.288 + 0.882 \log Z + 0.108 (\log Z)^2 \quad (1)$$

$$M_i = \begin{cases} 0.908 - 1.035 \log P + 0.220 \log Z, & \text{if RRab} \\ 0.908 - 1.035 (\log P + 0.128) + 0.220 \log Z, & \text{if RRc} \end{cases} \quad (2)$$

$$M_z = \begin{cases} 0.839 - 1.295 \log P + 0.211 \log Z, & \text{if RRab} \\ 0.839 - 1.295 (\log P + 0.128) + 0.211 \log Z, & \text{if RRc} \end{cases} \quad (3)$$

The M_v is by Catelan *et al.* (2004), and the M_i and M_z are by Cáceres and Catelan (2008). The $\log Z$ is a term related to a star's metallicity

$$\log Z = [M/H] - 1.765 \quad (4)$$

found by Catelan *et al.* (2004) and Cáceres and Catelan (2008), with

$$[M/H] = [Fe/H] + \log (0.638 \times 10^{0.3} + 0.362) \quad (5)$$

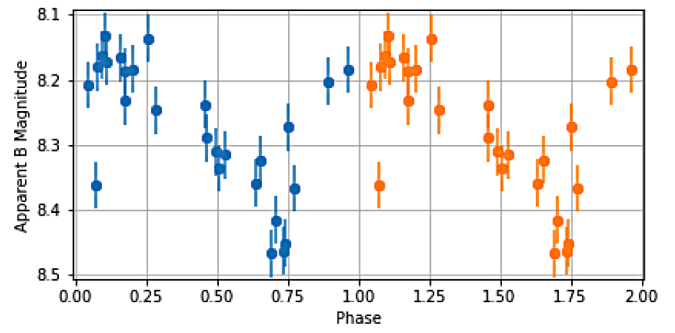


Figure 2. B light curve phase-plotted over two cycles and for the average period of 0.3705 day.

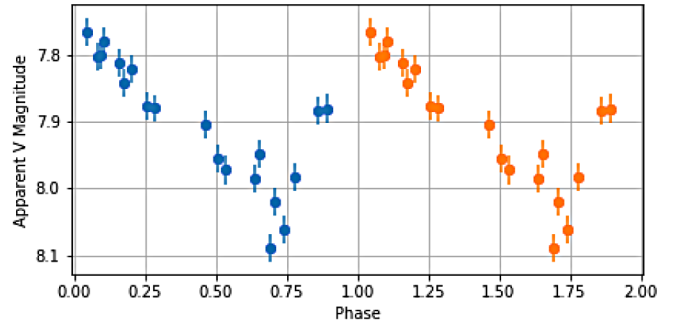


Figure 3. V light curve phase-plotted over two cycles and for the average period of 0.3705 day.

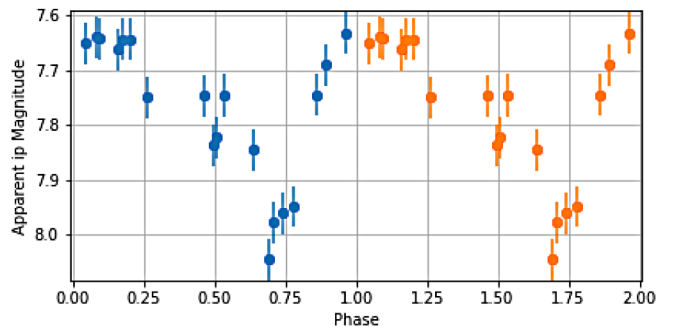


Figure 4. i light curve phase-plotted over two cycles and for the average period of 0.3705 day.

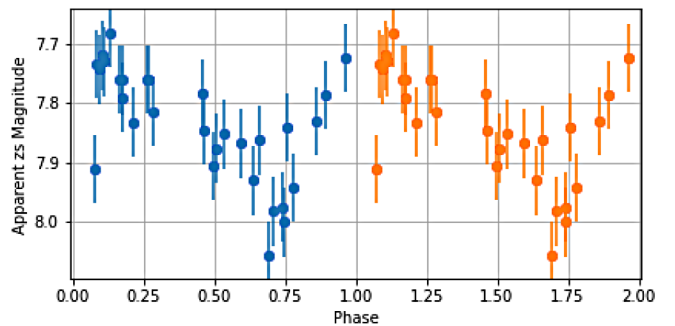


Figure 5. z light curve phase-plotted over two cycles and for the average period of 0.3705 day.

obtained by Salaris *et al.* (1993) and Cáceres and Catelan (2008). The goal is to calculate the star's absolute magnitudes and from them its distance. V350 Mus is a relatively metal-rich star, $10^{0.14} = 1.38$ times more metallic than the sun. With its metallicity being $[Fe/H] = 0.14$ (Table 1), Equation 5 gives $[M/H] = 0.354$ and Equation 4, $\log Z = -1.411 \pm 0.155$. Using the

average period $P=(0.3705\pm 0.0012)$ d, (Table 2), and that V350 Mus is an RRab, Equations 1, 2, and 3 are easily calculated, thus: $M_V=(1.258\pm 0.142)$ mag, $M_i=(1.044\pm 0.078)$ mag, and $M_z=(1.100\pm 0.068)$ mag.

These absolute magnitudes, together with the apparent magnitudes m (from Table 2), will lead us to the star's distance,

$$d = 10^{(m - M - A + 5) / 5} \quad (6)$$

provided that we first adjust the measured apparent magnitudes of each passband by the extinction factor A in order to account for interstellar reddening. A , in essence, puts the scattered starlight back into the apparent magnitude m —or equivalently, reduces the absolute magnitude M , in order to balance it with the observed m . The visual extinction to reddening ratio is

$$R_V \equiv \frac{A_V}{E(B-V)} \quad (7)$$

and the usually assumed standard value for the Milky Way is $R_V=3.1$. Furthermore, the mean reddening $E(B-V)$, from the galactic dust within a radius of 5 arcmin in the vicinity of V350 Mus (although not exactly along the line of sight to the star), is reported by the Schegel Dust Map service (NASA/IPAC 2020) to be (0.1738 ± 0.0032) mag. With these data we proceeded to calculate the star's distance for the V-, i-, and z-bands and then find the three-band average (d-viz-avg) based on five different calibration methods of A (see the subsection below). For each calibration method the d-viz-avg was optimum (compared to the Gaia number of 165.34 parsecs) when $E(B-V)=0.200$ mag, a number we chose for being the approximate upper bound of 0.1738 mag, thus justifying reasonably the optimization of our result as we arrived at it within the context of the Schegel Dust Map measured value. By the way, ASAS-SN catalogues (Jayasinghe *et al.* 2019; Shappee *et al.* 2014) list $E(B-V)=0.202$ mag for V350 Mus, information which strengthens our own approximation choice of 0.200 mag.

3.3. The A factor calibration

The final step in calculating the distance (Equation 6) is the calibration of A . It attempts to restore each filter's m by putting a proportional amount of A back into it. That is (and having in mind, say, general solid particle scattering), more "blue" than "red" wavelengths must be restored, thus a calibrated value of A has to be bigger for the shorter wavelengths.

To calibrate A we first write its un-calibrated expression and value:

$$A_{\text{un-cal}} = R_V \times E(B-V) = 3.100 \times 0.200 \text{ mag} \quad (8)$$

We propose to first calibrate A with a new extinction model, as follows:

$$A_{\text{cal}} = R_V E(B-V) \times \frac{\lambda_{\text{cal}}}{\lambda_b} \quad (9)$$

where λ_{cal} is a calibration wavelength (to be chosen below) and λ_b is the telescope's band wavelength center (the λ -ctr in Table 2)

for the V-, i-, and z-bands. So, parenthetically, if λ_b is the λ_v , λ_i , or λ_z , the exact notation of A_{cal} is really A_v , A_i , or A_z . Note that A_{cal} is chosen to be inversely proportional to λ_b in order to ensure that the "bluer" the wavelength is, the bigger A_{cal} is. This means that the amount of "blue" (short wavelength) which is restored in a corresponding blue apparent magnitude is more than the amount of "red" (long wavelength) which is restored in a corresponding red apparent magnitude, a restoration process which is reasonable since, generally, more blue than red scatters off the main beam of starlight on its way to the telescopes. Thus, Equation 9 attempts to restore a truer (more accurate) value of m for each wavelength and consequently a more precise value of distance.

Our proposed extinction model (Equation 9) will be implemented in four calibration methods and its results will then be compared to a fifth calibration method of another model which uses an actual interstellar extinction relation, one developed by Cardelli *et al.* (1989). Specifically, Tables 3.1, 3.2, 3.3, 3.4, and 3.5 show the distance results when reddening and extinction are taken into consideration for each of the following five calibration methods of A_{cal} (each of which has a unique λ_{cal}), respectively:

(1) $\lambda_{\text{cal}} = \lambda_v$ where $\lambda_v = 5448 \text{ \AA}$. The results are in Table 3.1.

(2) $\lambda_{\text{cal}} = \lambda_{\text{mean}}$ where

$$\lambda_{\text{mean}} = (\lambda_v + \lambda_i + \lambda_z) / 3 = (5448 + 7545 + 8700) / 3 = 7231 \text{ \AA}.$$

The results are in Table 3.2.

(3) $\lambda_{\text{cal}} = \lambda_{\text{weighted-mean}} \equiv \lambda_{w\text{-mean}}$ where

$$\lambda_{w\text{-mean}} = \frac{\sum_b^{V,i,z} w_b \lambda_b}{\sum_b^{V,i,z} w_b} = \frac{w_v \lambda_v + w_i \lambda_i + w_z \lambda_z}{w_v + w_i + w_z} \quad (10)$$

with weight coefficients (of each band wavelength)

$$w_b \equiv \frac{\lambda_b}{\lambda_{\text{ref}}} \quad (11)$$

and where λ_{ref} is an arbitrary reference wavelength that cancels out in the determination of $\lambda_{w\text{-mean}}$. That is, using Equation 11, Equation 10 becomes

$$\lambda_{w\text{-mean}} = \frac{\lambda_v^2 + \lambda_i^2 + \lambda_z^2}{\lambda_v + \lambda_i + \lambda_z} \quad (12)$$

Then, using each band's wavelength center, $\lambda_v = 5448 \text{ \AA}$, $\lambda_i = 7545 \text{ \AA}$, and $\lambda_z = 8700 \text{ \AA}$, Equation 12 yields $\lambda_{w\text{-mean}} = 7482 \text{ \AA}$. Thus for method (3) $\lambda_{\text{cal}} = 7482 \text{ \AA}$, and the consequent results are shown in Table 3.3.

(4) For calibration method (4) the weight coefficients, Equation 11, are

$$w_b \equiv \frac{I(\lambda_b)}{I(\lambda_{\text{ref}})} \quad (13)$$

Table 3.1. Distance based on reddening $E(B-V) = 0.200$ mag and A calibration $\lambda_{\text{cal}} = \lambda_V = 5448 \text{ \AA}$.

	V	$\text{Band } i$	z
A_{cal} (mag)	0.620	0.448	0.388
d (parsec)	162.09	185.91	188.90
errd (parsec)	12	8	7
d-viz-avg (parsec)		178.97 \pm 5	
% diff ^g		8.24	

^gBetween d-viz-avg and Gaia's 165.34 parsecs.Table 3.2. Distance based on reddening $E(B-V) = 0.200$ mag and A calibration $\lambda_{\text{cal}} = \lambda_{\text{mean}} = 7231 \text{ \AA}$.

	V	$\text{Band } i$	z
A_{cal} (mag)	0.823	0.594	0.515
d (parsec)	147.63	173.79	178.17
errd (parsec)	11	7	7
d-viz-avg (parsec)		166.53 \pm 5	
% diff ^g		0.72	

^gBetween d-viz-avg and Gaia's 165.34 parsecs.Table 3.3. Distance based on reddening $E(B-V) = 0.200$ mag and A calibration $\lambda_{\text{cal}} = \lambda_{\text{w-mean-method-3}} = 7482 \text{ \AA}$.

	V	$\text{Band } i$	z
A_{cal} (mag)	0.851	0.615	0.533
d (parsec)	145.70	172.14	176.70
errd (parsec)	11	7	7
d-viz-avg (parsec)		164.85 \pm 5	
% diff ^g		0.30 ^a	

^gBetween d-viz-avg and Gaia's 165.34 parsecs. ^aor 0.01% when $E(B-V) = 0.198$. Incidentally, when $\lambda_{\text{cal}} = \lambda_i = 7545 \text{ \AA}$ and $E(B-V) = 0.196$ mag, the percent difference of the d-viz-avg (from the Gaia distance) is also low, 0.05%, but we think this is so because λ_i happens to accidentally be approximately equal to $\lambda_{\text{w-mean}} = 7482 \text{ \AA}$.Table 3.4. Distance based on reddening $E(B-V) = 0.200$ mag and A calibration $\lambda_{\text{cal}} = \lambda_{\text{w-mean-method-4}} = 6686 \text{ \AA}$.

	V	$\text{Band } i$	z
A_{cal} (mag)	0.761	0.549	0.476
d (parsec)	151.91	177.40	181.38
errd (parsec)	11	7	7
d-viz-avg (parsec)		170.23 \pm 5	
% diff ^g		2.96	

^gBetween d-viz-avg and Gaia's 165.34 parsecs.Table 3.5. Distance based on reddening $E(B-V) = 0.200$ mag and A calibration method (5) (Cardelli *et al.* 1989).

	V	$\text{Band } i$	z
A_{cal} (mag)	0.620	0.424	0.305
d (parsec)	162.09	187.95	196.28
errd (parsec)	12	8	7
d-viz-avg (parsec)		182.11 \pm 5	
% diff ^g		10.14	

^gBetween d-viz-avg and Gaia's 165.34 parsecs.

where

$$I(\lambda) = \frac{2hc}{\lambda^3} \frac{1}{e^{hc/\lambda kT} - 1} \quad (14)$$

is the star's black-body radiation intensity. For method (4) Equation 10 becomes

$$\lambda_{\text{w-mean}} = \frac{I(\lambda_V)\lambda_V + I(\lambda_i)\lambda_i + I(\lambda_z)\lambda_z}{I(\lambda_V) + I(\lambda_i) + I(\lambda_z)} \quad (15)$$

With $T = T_{\text{eff}} = 6356.19 \text{ K}$ (Table 1), Equation 15 gives $\lambda_{\text{w-mean}} = 6686 \text{ \AA}$. Thus $\lambda_{\text{cal}} = 6686 \text{ \AA}$, and the corresponding results are shown in Table 3.4.Note that λ_{mean} (from method 2) and $\lambda_{\text{w-mean}}$ (from methods 3 and 4) were calculated using only the V-, i-, and z-bands (but not the B), as only these bands have a formula for M (and thus indirectly distance), their results of which can be compared against each other (as well as against the Gaia distance) in order to determine the effectiveness of each calibration method.(5) Lastly, calibration method (5), developed by Cardelli *et al.* (1989), yields the results of Table 3.5. For calibration (5), Equation 9 is replaced by

$$A_{\text{cal}} = R_V \times E(B-V) \times f \quad (16)$$

where the factor f is obtained when Equations 2 and 3 from Cardelli *et al.* (1989) are used for the V, i, and z wavelengths.

3.4. Distance results

Tables 3.1, 3.2, 3.3, 3.4, and 3.5 include the distance results with reddening and A calibration via methods (1), (2), (3), (4), and (5), respectively. The best d-viz-avg result, having only a 0.30% difference from the Gaia distance (Table 3.3), was obtained by method (3), a weighted-mean calibration of A.

4. Discussion

The main goal of the paper was to test the validity of three period-luminosity-metallicity relations (Equations 1, 2, 3) against observational data obtained from a single star, V350 Mus. The formulas performed quite well since, collectively, they generated a three-filter average distance that, within the margin of error, agrees with the Gaia distance (see Table 3.3, or Table 4 which summarizes the main results). The individual distances from the data of the i and z filters were

within each other’s margin of error but not with the distance value from the V filter. Also, the M_i and M_z formulas performed better than the M_v (in matching the Gaia distance)—probably an indication that the M_v formula needs further refinement. These results are expected within the context of Catelan *et al.* (2004), where the period-luminosity graph in the i filter shows a narrower spread of points (a sharper line with less noise, thus a more accurate M_i expression), but a rather scattered spread of points in the V filter (thus a less accurate M_v expression)—V350 Mus might be an example of the scattered V points. (That paper does not include a z filter graph.)

Using the Sloan Digital Sky Survey (SDSS) photometric system, Cáceres and Catelan (2008), too, has a low noise graph in the i filter, but also in the z filter (meaning that, the M_i and M_z formulas are generally expected to outperform the M_v formula, as verified by our study). Recall, Equation 1 is from Catelan *et al.* (2004) and Equations 2 and 3 are from Cáceres and Catelan (2008). Hence our distance results confirm rather well the theoretical predictions of those papers.

If these formulas are verified further by similar research involving many other stars, they could be used in “reverse”: for example, from the known distance and metallicity of an RR Lyrae star and by measuring its period and m, we can calculate A using

$$M = m - A + 5 - 5 \log d \quad (17)$$

and thus determine a star’s reddening value $E(B-V)$. That is important as the reddening values reported by the Schegel Dust Map are generally approximations in the general vicinity of a star. Or, in another example for these formulas’ usage, we could determine a star’s metallicity if we knew its reddening and distance, and measured its m and period.

Interestingly, our simple calibration formula, Equation 9, implemented in methods 1-4, produced better distance results in every case (as seen in Tables 3.1, 3.2, 3.3, and 3.4), compared to the more complex calibration method (5) found in Cardelli *et al.* (1989) (as seen in Table 3.5). The reason for this might be that, in the accounting of the phenomenon of extinction, our approach considers the amount of each wavelength’s extinction proportionally, by balancing it with respect to the extinction of an average wavelength (as seen specifically in Tables 3.2, 3.3, and 3.4), whereas the paper by Cardelli *et al.* (1989) arrives at its extinction formulas by calibrating a wavelength’s extinction with respect to the extinction of only the V wavelength. The hypothesis that such a simple calibration formula, Equation 9, can produce good distance results (via methods 1-4) is worth testing further.

Based on the results of Tables 3.1, 3.2, 3.3, 3.4, and 3.5 we propose that the best calibration method for the extinction factor A is Equation 9 implemented via method (3), Equation 10, the weighted-mean of the wavelengths that have a period-luminosity-metallicity relation (and are used in the observations), along with Equation 11. Recall that in that case (Table 3.3 or 4), the percent difference between the Gaia value of distance and our value was only 0.30% when $E(B-V) = 0.200$ (or 0.01% when $E(B-V) = 0.198$). This hypothesis can be tested by imaging a star in as many wavelengths as possible,

Table 4. V350 Mus Summary of Main Results: $E(B-V) = 0.200$ mag; A is calibrated with $\lambda_{\text{cal}} = \lambda_{w-\text{mean}-\text{method}-3} = 7482 \text{ \AA}$.

	V	Band i	z
d (parsec)	145.70	172.14	176.70
errd (parsec)	11	7	7
d-viz-avg (parsec)		164.85 ± 5	
d-Gaia (parsec)		165.34 ± 1	
% diff ^a		0.30 ^a	
P (d)		0.3705 ± 0.0012	
V350 Mus		RRab (reclassified)	

^a Between d-viz-avg and the Gaia distance. ^aor 0.01% when $E(B-V) = 0.198$.

as long as each of these wavelengths has also a corresponding period-luminosity-metallicity relation.

Lastly, we discovered that V350 Mus is an RRab type. Prior to this research the star was classified as either an RRc (Watson *et al.* 2006; Kazarovets *et al.* 2011; Samus *et al.* 2017), or an eclipsing variable (EW) (Watson *et al.* 2014; Astraatmadja and Bailer-Jones 2016). The calculated amplitudes (Table 2) were not clearly telling of the type of RR Lyrae star V350 Mus is, as these values were roughly between those typical of an RRc type (which are usually of lower amplitudes) and those typical of an RRab type (which are usually of higher amplitudes). However, the four light curves (Figures 2–5) clearly reclassified V350 Mus as an RRab: one can see a sharper ascent with a more gradual descent in the luminosity cycle, characteristic of RRab stars. An additional piece of evidence that reinforces the star’s reclassification is this: when the period-luminosity-metallicity relations (Equations 1, 2, 3) are evaluated by assuming an RRc type star then all distance results—i. e., what Tables 3.1, 3.2, 3.3, 3.4, and 3.5 would be like in such case—are worse compared to the only reported star distance, that of Gaia.

The period we measured, 0.3705 d (Table 2), is in quite good agreement with one of the reported periods, 0.36905 d (Table 1), its reference of which had classified the star as an RR Lyrae star (although of type RRc). However, our study’s period doesn’t agree with the other reported period, 0.73811 d (Table 1), its reference of which had classified the star as an EW type. Thus, the period analysis is additional evidence that V350 Mus is an RR Lyrae type star, and not an EW. Moreover, V350 Mus’s reclassification to RRab is supported by yet more evidence related to the star’s short period and relatively high metallicity, because short period and high metallicity are general characteristics of RRab variables, not of RRc. RRc variables with metallicity as high as that of V350 Mus are considered rare.

Another general characteristic, typical of an RR Lyrae star light curve, is a bump along the descent of the curve. Although not very clear, a tiny bump does exist in the descent of at least some of the light curves in our study. This feature together with the period agreement (mentioned above) solidify the star’s reclassification as an RR Lyrae variable instead of an eclipsing variable (from a previous classification).

5. Conclusion

We measured the period and apparent magnitude of V350 Mus. We inserted the period and the star’s metallicity

in three theoretical period-luminosity-metallicity relations (M_V , M_i , and M_z) in order to calculate the star's absolute magnitude in the corresponding filters. We then adjusted the apparent magnitude of each filter by adding to it an extinction factor, calculated each filter's distance, and, by comparing the results with one another, as well as comparing the three-filter average distance with the Gaia distance, we were able to check the validity of the theoretical period-luminosity-metallicity relations. Collectively, the relations performed quite well in the case study of a single star, V350 Mus.

The distances (in parsecs) were estimated to be: 145.70 ± 11 in the V filter; 172.14 ± 7 in i; and 176.70 ± 7 in z. The three-filter average distance is 164.85 ± 5 , only 0.30% difference from the Gaia value of 165.34 ± 1 . The pulsation period was 0.3705 ± 0.0012 day.

The average distance was optimum when the extinction factor was calibrated using a new simpler method, which involved the weighted mean of the band wavelengths that had a period-luminosity-metallicity relation (the V, i, and z wavelengths in our case), and where the weight of a particular band wavelength was its ratio to an arbitrary reference wavelength. This method did better compared to the older method by Cardelli *et al.* (1989). We hope to test the effectiveness of the new calibration method further in a future study. The present research reclassified V350 Mus as an RRab Lyrae type.

6. Acknowledgements

We are grateful to Dr. Michael Fitzgerald for his continuous support and valuable advice during every step of this project. We also thank Dr. Brian Uzpen for connecting us to MF. We are also indebted to both the JAAVSO editor and the anonymous referee whose comments and suggestions have undoubtedly improved the quality of the manuscript.

DN thanks Bloomfield College's PBI office for funding. DN and DK thank Bloomfield College's McNair Program office for funding.

References

- Altunin, I., Caputo, R., and Tock, K. 2020, *Astron. Theory, Obs., Methods*, **1**, 1.
- Ammons, S. M., Robinson, S. E., Strader, J., Laughlin, G., Fischer, D., and Wolf, A. 2006, *Astrophys. J.*, **638**, 1004.
- Astraatmadja, Tri L., and Bailer-Jones, C. A. L. 2016, *Astrophys. J.*, **833**, 119.
- Bailer-Jones, C. A. L., Rybizki, J., Foesneau, M., Mantelet, G., and Andrae, R. 2018, *Astron. J.*, **156**, 58.
- Bertin, E., and Arnouts, S. 1996, *Astron. Astrophys., Suppl. Ser.*, **117**, 393.
- Bonnarel, F., *et al.* 2000, *Astron. Astrophys., Suppl. Ser.*, **143**, 33.
- Brown, T., *et al.* 2013, *Publ. Astron. Soc. Pacific*, **125**, 1031.
- Cáceres, C., and Catelan, M. 2008, *Astrophys. J., Suppl. Ser.*, **179**, 242.
- Cardelli, J. A., Clayton, G. C., and Mathis, J. S. 1989, *Astrophys. J.*, **345**, 245.
- Catelan, M., Pritzl, B. J., and Smith, H. A. 2004, *Astrophys. J., Suppl. Ser.*, **154**, 633.
- Catelan, M., and Smith, H. A. 2014, *Pulsating stars*, John Wiley and Sons, Hoboken, NJ.
- Collins, K. A., Kielkopf, J. F., Stassun, K. G., and Hessman, F. V. 2017, *Astron. J.*, **153**, 77.
- Dworetzky, M. 1983, *Mon. Not. Roy. Astron. Soc.*, **203**, 917.
- Fitzgerald, M. 2018, in *Robotic Telescope, Student Research and Education Proceedings, Vol. 1, No. 1*, RTSRE, San Diego, CA, 347.
- Gaia Collaboration, Brown, A., *et al.* 2018, *Astron. Astrophys.*, **616A**, 1.
- Gaia Collaboration, Clementini, G., *et al.* 2017, *Astron. Astrophys.*, **605A**, 79.
- Henden, A. A., Templeton, M., Terrell, D., Smith, T. C., Levine, S., and Welch, D. 2016, *VizieR Online Data Catalog: AAVSO Photometric All Sky Survey (APASS) DR9*, II/336.
- Høg, E., *et al.* 2000, *The Tycho-2 Catalogue of the 2.5 Million Brightest Stars*, *Astron. Astrophys.*, **355**, L27.
- Hubble, E. 1929, *Proc. Natl. Acad. Sci. USA*, **15**, 168.
- Jayasinghe, T., *et al.* 2019, *Mon. Not. Roy. Astron. Soc.*, **485**, 961.
- Kazarovets, E. V., Samus, N. N., Durlevich, O. V., Kireeva, N. N., and Pastukhova, E. N. 2011, *Inf. Bull. Var. Stars*, No. 6008, 1.
- Leavitt, H. S. 1908, *Ann. Harvard Coll. Obs.*, **60**, 87.
- NASA/IPAC Infrared Science Archive (IRSA). 2020, *Galactic Dust Reddening and Extinction* (<https://irsa.ipac.caltech.edu/applications/DUST>).
- Salaris, M., Chieffi, A., and Straniero, O. 1993, *Astrophys. J.*, **414**, 580.
- Samus, N. N., Kazarovets, E. V., Durlevich, O. V., Kireeva, N. N., and Pastukhova, E. N. 2017, *Astron. Rep.*, **61**, 80.
- Schlafly, E. F., Meisner, A. M., and Green, G. M. 2019, *Astrophys. J., Suppl. Ser.*, **240**, 30.
- Shappee, B. J., *et al.* 2014, *Astrophys. J.*, **788**, 48.
- Stellingwerf, R. F. 1978, *Astrophys. J.*, **224**, 953.
- Watson, C. L., Henden, A. A., and Price, A. 2006, in *The Society for Astronomical Sciences 25th Annual Symposium on Telescope Science*, Society for Astronomical Sciences, Rancho Cucamonga, CA, 47.
- Watson, C., Henden, A. A., and Price, C. A. 2014, *AAVSO International Variable Star Index VSX (Watson+, 2005–2020)*; <https://www.aavso.org/vsx>.
- Wolf, C., *et al.* 2018, *Publ. Astron. Soc. Australia*, **35**, 10.